Journal of the Serbian Chemical Society
JSCS@tmf.bg.ac.rs • www.shd.org.rs/JSCS
J. Serb. Chem. Soc. *90* (9) 1089–1104 (2025)
JSCS–5441
Original scientific paper
Published 30 September, 2025

Water-splitting electrocatalytic properties and computational characterization of a symmetrically substituted porphyrazine

MARINA ALEXANDRA TUDORAN and BOGDAN-OVIDIU TARANU*

National Institute of Research and Development for Electrochemistry and Condensed Matter, Dr. A. Paunescu Podeanu Street No. 144, 300569 Timisoara, Romania

(Received 23 March, revised 19 June, accepted 10 July 2025)

Abstract: The porphyrazine 2,7,12,17-tetra-*tert*-butyl-5,10,15,20-tetraaza-21*H*,23*H*-porphine was studied regarding its electrocatalytic water-splitting activity in a wide pH range. Two different methods were employed to manufacture electrodes based on this compound: a solution-based method and a catalyst ink-based one. The most catalytically active electrode was obtained using the catalyst ink-based method. In 1 mol L^{-1} KOH solution it displays an H_2 evolution reaction overpotential of 0.6 V and a Tafel slope of 0.15 V dec^{-1}. Statistical analysis revealed a significant correlation between the pH and the O_2 evolution reaction overpotential. Quantum chemical calculations were performed to obtain a more detailed understanding of the porphyrazine's properties.

Keywords: electrocatalyst; hydrogen evolution reaction; oxygen evolution reaction; quantum chemical calculations; correlation analysis.

INTRODUCTION

Porphyrins, corroles, phthalocyanines, naphthalocyanines, subphthalocyanines and porphyrazines are classes of tetrapyrrole macrocyclic organic compounds and members of the porphyrinoids family.[1] Of these, porphyrazines, also known as tetraazaporphyrins, exhibit features differentiating them from porphyrins by having nitrogen atoms in the *meso*-positions of their macrocycle instead of carbon atoms, and from phthalocyanines by having their *β*-pyrrole positions available for functionalization.[2] Concerning their applications, these compounds are being studied as photosensitizers for photodynamic therapy and dye-sensitized solar cells, as photocatalysts, electrocatalysts, as well as fluorescent and optical sensors.[3–7] 2,7,12,17-Tetra-*tert*-butyl-5,10,15,20-tetraaza-21*H*,23*H*-porphine is a member of the tetraazaporphyrin class that has been the subject of some reported studies.[8–12] However, no published investigation regarding the electrocatalytic water-splitting

* Corresponding author. E-mail: b.taranu84@gmail.com
https://doi.org/10.2298/JSC250323043T

properties of this particular porphyrazine has been identified. Revealing the hydrogen evolution reaction catalytic activity of electrode materials is of appreciable current importance. Presently, green hydrogen generated via renewable energy-based water-splitting is highly desirable in the global effort of diminishing greenhouse gas emissions.[13] Considerable efforts to decrease greenhouse gas emissions, to slow down global warming and to contain the accelerated climate change are currently being made by many countries.[14] Different technologies are available for hydrogen generation through water-splitting,[15] but electrochemical water-splitting is one of the most promising for the production of green hydrogen.[16] The main reactions occurring during water electrolysis are the oxygen evolution reaction (OER) at the anode and the hydrogen evolution reaction (HER) at the cathode.[17] The former is the major bottleneck of the whole process due its sluggish electrochemical kinetics.[18] The benchmark electrocatalysts for the two reactions are Ir/Ru and Pt-based electrode materials.[19] Due to the scarcity and high costs characteristic of noble metals, it is difficult to use such materials for large-scale water-splitting. As a result, researchers have been investigating other compounds with electrocatalytic properties, either based on low-cost, Earth-abundant transition metals or metal-free carbon-based ones.[20–22] Regarding porphyrazines, even though no reported study of the water electrolysis activity of 2,7,12,17-tetra-*tert*-butyl-5,10,15,20-tetraaza-21*H*,23*H*-porphine was found, there are other members of the porphyrazine class that have been investigated as noble metal-free water-splitting electrocatalysts.[6]

The current work describes two investigations. One of them is experimental, while the other is theoretical. The experimental study concerns the electrochemical water-splitting activity of the aforementioned compound in a wide pH range by using porphyrazine-modified electrodes manufactured via different protocols. The theoretical part consists of quantum chemical calculations of the porphyrazine molecule in gas phase using three different hybrid density functional theory (DFT) methods, as well as statistical analysis. Although the computational modeling and experimental investigation are based on different principles, they are complementary methods which can provide a deeper understanding of the compound's structure and properties.

EXPERIMENTAL

Materials and reagents

2,7,12,17-Tetra-*tert*-butyl-5,10,15,20-tetraaza-21*H*,23*H*-porphine (Scheme S-1 of the Supplmentary material) was purchased from Sigma–Aldrich and used as received. The following organic solvents were procured and used to obtain the tetraazaporphyrin solutions: *N*,*N*-dimethylformamide (DMF), acetonitrile (CH_3CN), benzonitrile (PhCN), ethanol (EtOH), tetrahydrofuran (THF) and dichloromethane (DCM) from Sigma–Aldrich, Honeywell (Charlotte, NC, USA) and Merck. Nafion® 117 solution and carbon black, Vulcan® XC 72 were purchased

from Sigma–Aldrich and Fuell Cell Store (Bryan, TX, USA) and used to prepare the tetraazaporphyrin suspensions. The solid substrates utilized to manufacture the electrodes were glassy carbon (GC) tablets (∅ 8 mm) obtained from Andreescu Labor & Soft SRL (Bucharest, Romania). Sulfuric acid 98 %, potassium chloride and potassium hydroxide were procured from Merck to prepare the electrolyte solutions. All reagents were used as received and all electrolyte solutions were obtained with double-distilled water from a water double distillation unit (Fistreem, Cambridge, UK).

Electrode manufacturing methods

Two different methods were employed to obtain the porphyrazine-modified electrodes used in the electrochemical experiments aimed at evaluating the compound's water-splitting electrocatalytic properties. Regarding the first method, the tetraazaporphyrin was dissolved in organic solvents with different polarity, increasing as follows: DCM < THF < EtOH < PhCN < CH_3CN < DMF.[23,24] The solutions were utilized to modify the surface of the GC tablets *via* the drop-casting technique. A volume of 10 μL was applied to obtain one porphyrazine layer. After solvent evaporation at 40 °C a modified substrate was either used as an electrode in the electrochemical experiments or it was further modified with one or two more layers. The names of the electrodes are presented in Table I along with the solvents employed to dissolve the traazaporphyrin and the number of layers deposited on the GC support.

TABLE I. Names of porphyrazine-modified electrodes obtained with the solution-based method

Electrode name	Solvent	Porphyrin layers	Electrode name	Solvent	Porphyrin layers
$GC_{AP\text{-}DCM\text{-}1}$	DCM	1	$GC_{AP\text{-}PhCN\text{-}1}$	PhCN	1
$GC_{AP\text{-}DCM\text{-}2}$		2	$GC_{AP\text{-}PhCN\text{-}2}$		2
$GC_{AP\text{-}DCM\text{-}3}$		3	$GC_{AP\text{-}PhCN\text{-}3}$		3
$GC_{AP\text{-}THF\text{-}1}$	THF	1	$GC_{AP\text{-}CH3CN\text{-}1}$	CH_3CN	1
$GC_{AP\text{-}THF\text{-}2}$		2	$GC_{AP\text{-}CH3CN\text{-}2}$		2
$GC_{AP\text{-}THF\text{-}3}$		3	$GC_{AP\text{-}CH3CN\text{-}3}$		3
$GC_{AP\text{-}EtOH\text{-}1}$	EtOH	1	$GC_{AP\text{-}DMF\text{-}1}$	DMF	1
$GC_{AP\text{-}EtOH\text{-}2}$		2	$GC_{AP\text{-}DMF\text{-}2}$		2
$GC_{AP\text{-}EtOH\text{-}3}$		3	$GC_{AP\text{-}DMF\text{-}3}$		3

The solution-based GC modification strategy relies on the fact that porphyrazine molecules are capable of spontaneous self-assembly through non-covalent interactions into supramolecular aggregates.[25,26] Typically, the properties of these aggregates are different than those of the individual molecules.[27] The aggregation behavior depends on several factors, such as solvent type, the amount of material, the type of substituents, the presence or absence of a central metal ion, the surrounding environment (*e.g.*, the solid support and the atmosphere) and temperature.[26] The electrodes were manufactured by varying the solvent type and the number of deposited layers in the case of each solvent.

The second method employed to obtain tetraazaporphyrin-modified electrodes is the catalyst ink-based method.[28] The inks were obtained by dispersing in water an amount of porphyrazine or of porphyrazine and carbon black during a 30-min ultrasonication stage. The surface of the solid supports was modified by drop-casting a catalyst ink volume of 10 μL. The modified supports were dried at 40 °C and the resulting samples were used as electrodes in the electrochemical experiments. Table II shows the names of the electrodes and the compositions of the catalyst inks.

TABLE II. Names of porphyrazine-modified electrodes obtained with the catalyst ink-based method

Electrode name	Porphyrin amount mg	Carbon black mg	Nafion solution μL	Double-distilled water μL
GC_{AP}	10	–	50	450
GC_{CB-AP}	5	5	50	450

Electrochemical experiments

The setup used to perform the electrochemical investigations consisted of a standard glass cell for electrochemical experiments containing the electrolyte solution, a potentiostat (Voltalab, model PGZ 402, from Radiometer Analytical, Lyon, France) and three electrodes that were connected to the device and inserted into the solution. The auxiliary electrode was a Pt plate having a geometric surface (S_{geom}) of 0.8 cm^2. The Ag/AgCl (sat. KCl) electrode was utilized as reference electrode. The working electrode was each of the tetraazaporphyrin-modified electrodes after being placed inside a polyamide support that restricted the area exposed to the electrolyte solution to S_{geom} = 0.28 cm^2. To cover a wide pH range, the following electrolyte solutions were employed in the study: 0.1 mol L^{-1} KCl, 0.1 mol L^{-1} H_2SO_4, and 1 mol L^{-1} KOH. Before the HER experiments, the electrolyte solutions were bubbled with high-purity N_2. The linear sweep voltammograms (LSVs) obtained during the HER and OER tests were *IR*-corrected and their recording was carried out at a 5 mV s^{-1} scan rate (v).[29] The parameter j represents the geometric current density, while E is the electrochemical potential *vs.* reversible hydrogen electrode (RHE). The equations used to express the potential *vs.* the specified reference electrode, to calculate the oxygen and hydrogen evolution overpotentials (η_{OER} and η_{HER}) and the Tafel equation can be found in the Supplementary material as Eqs. (S-1), (S-2), (S-3) and (S-4), respectively.[30-32] Eqs. (S-5) and (S-6) are also relevant to the electrochemical study, as outlined in the Results and Discussion section.

Raman spectroscopy analysis

Raman spectra were recorded using a MultiView-2000 system (Nanonics Imaging Ltd., Jerusalem, Israel) with a Shamrock 500i spectrograph (Andor, Essex, UK).

Theoretical calculations

Quantum chemical calculations for the tetraazaporphyrin in the ground state were carried out using HyperChem 8.1 and Gaussian03 software. Pre-optimization of the molecule was conducted using HyperChem and the semi-empirical PM3 model. The obtained molecular configuration was then subjected to further optimization with the Gaussian 03 in DFT framework, without symmetry constraints, using the Becke 3-Lee-Yang-Parr (B3LYP), B3PW91 and MPW1PW91 functionals with STO-3G basis set. To verify that the obtained structure corresponds to a minimum on the potential energy surface, frequency calculations were performed at the same theoretical levels. Single point calculations were performed using 6-31G(d) basis set. Gaussian output files were visualized using Gauss View 6.0 software. A statistical analysis was performed using IBM SPSS 21 to ascertain the association between the studied electrochemical parameters.

RESULTS AND DISCUSSION

Results of the quantum chemical calculations

The structural parameters calculated with B3LYP/STO-3G, B3PW91/STO--3G and MPW1PW91/STO-3G are presented in Table S-I of the Supplementary material. Data obtained by Mongale *et al.* for the unfunctionalized porphyrazine were used for comparison.[33] The results obtained show that, with the exception of the C_{19}–C_{17} and C_{15}–C_{20} bonds, the carbon bond lengths for tetraaza-porphyrin were slightly higher than those of the unfunctionalized porphyrazine. In contrast, the values of the angles between carbon and nitrogen atoms were lower in the case of the tetraazaporphyrin, with the exception of the C_{15}–N_{21}–C_{13}, which was found to be lower in the case of the unfunctionalized porphyrazine. These variations arise from the alteration of the macrocycle's geometry, which occurs due to its functionalization with tert-butyl groups. The optimized structures for the tetraazaporphyrin and atom numbering are shown in Fig. S-1 of the Supplementary material.

The chemical activity of the compound was evaluated by examining the highest occupied molecular orbital (HOMO) and lowest unoccupied molecular orbital (LUMO) frontier molecular orbitals. The HOMO energy is indicative of the molecule's capacity to donate electrons in a chemical reaction, while the LUMO energy is indicative of its capacity to accept electrons.[33] The energy gap between the HOMO and LUMO energies denotes the energy required for a molecule to transition from the ground state to an excited state, being a critical factor in determining its reactivity tendency, optical polarizability, and kinetic stability.[34,35] The spatial distribution of the HOMO and LUMO orbitals and the corresponding energies are shown in Fig. S-2 and Table S-II of the Supplementary material. The HOMO and LUMO orbitals for the tetraazaporphyrin are localized at the carbon atoms of the macrocycle, which is similar to the unfunctionalized porphyrazine.[34] However, the value of the energy gap is slightly smaller, 2.303 (B3LYP/6-31G(d)), 2.538 (B3PW91/6-31G(d)) and 2.331 (MPW1PW91/6-31G(d)), compared to the 2.63 value reported by Mongale *et al.*[33] The vertical ionization potential and electron affinity for the tetraazaporphyrin were calculated using the ΔSCF formalism (Eqs. (S-7) and (S-8) from the Supplementary Material). The results are presented in Table S-II. The smallest values of both parameters were obtained with B3LYP/6-31G(d).

Table S-III of the Supplementary materialshows the values of the thermodynamic parameters. They can be used in calculating the Gibbs energy change, as part of the thermodynamic cycle,[36] and include the dipole moment, the zero-point vibrational energy, the sum of electronic energies with the zero-point correction and the thermal energy and enthalpy corrections. The rotational constants, thermal energy, heat capacity and entropy are also provided. Results indicate that the B3LYP/STO-3G method yields the highest values, except for the dipole moment,

zero-point vibrational energy, and thermal energy, for which higher values were obtained with the MPW1PW91/STO-3G method.

Natural charge, population and electronic configuration are commonly used to explain the electronic properties of molecules. Natural bond orbital (NBO) analysis was also employed to assess the nature of the bonding interaction with regard to charge transfer and orbital interactions, as well as to obtain a more comprehensive understanding of the dissociation process' activation.[37,38]

According to the results in Table S-IV of the Supplementary material, N atoms display only negative charges, H atoms display only positive charges and C atoms display both positive and negative charges – depending on the type of bonding they are involved in.

Polarizability and hyperpolarizability serve to characterize the response of a system to an applied electric field. Literature data indicates that organic molecules containing conjugated π-electrons exhibit high values of the first molecular hyperpolarizability.[39] It was also shown that increased polarization can result in enhanced adsorption, thereby decreasing surface adsorption resistance during the oxygen evolution reaction.[40] The complete set of equations employed for the calculation of the polarizability (α), the anisotropy of polarizability ($\Delta\alpha$), and the first hyperpolarizability (β) are available in the Supplementary material as Eqs. (S-9) to (S-11), with the results being presented in Table S-V of the Supplementary material. The highest polarizability values were obtained with the B3LYP/6--31G(d) method, while the highest hyperpolarizability value was acquired *via* the B3PW91/6-31G(d) method.

Experiments with electrodes obtained using the solution-based method

The results obtained by studying the water electrolysis catalytic activity of the electrodes manufactured with the solution-based method evidence the ways in which the organic solvents and the number of deposited tetraazaporphyrin layers influence the OER and HER overpotential values. The anodic polarization curves recorded in the acidic, neutral, and alkaline environments are presented in Figs. S-3, S-4 and S-5 of the Supplementary material. In most cases, the electrocatalytic activity of the porphyrazine-modified electrodes is lower than that of the unmodified GC electrode (GC_0). In the few situations in which it is higher the difference is not significant, with the exception of the $GC_{AP\text{-}PhCN\text{-}1}$ electrode immersed in 0.1 mol L^{-1} KCl solution (Fig. S-4a). When specifying the OER and HER overpotential values of different electrodes the current density value accepted as benchmark is 10 mA cm^{-2} for OER and −10 mA cm^{-2} for HER.[31] At this j value the η_{OER} for $GC_{AP\text{-}PhCN\text{-}1}$ and GC_0 is 1.24 and 1.32 V, respectively. As the current density increases this difference decreases until (at j = ~ 30 mA cm^{-2}) the η_{OER} value is the same for both specimens. Fig. S-6, S-7 and Fig. 1 show the cathodic polarization curves obtained on the electrodes manufactured with the solution-

based protocol in the 0.1 mol L^{-1} H_2SO_4, 0.1 mol L^{-1} KCl and 1 mol L^{-1} KOH electrolyte solutions. In the selected potential range only two electrodes display water-splitting electrocatalytic activity at −10 mA cm^{-2}: $GC_{AP\text{-}DMF\text{-}1}$ (η_{HER} = 0.916 V) and $GC_{AP\text{-}PhCN\text{-}3}$ (η_{HER} = 0.9 V). The LSVs for these specimens were recorded in the strong alkaline medium and can be seen in Fig. 1a and c, respectively. Out of the HER overpotential values determined for the electrodes obtained with the solution-based modification strategy the 0.9 V value is the lowest.

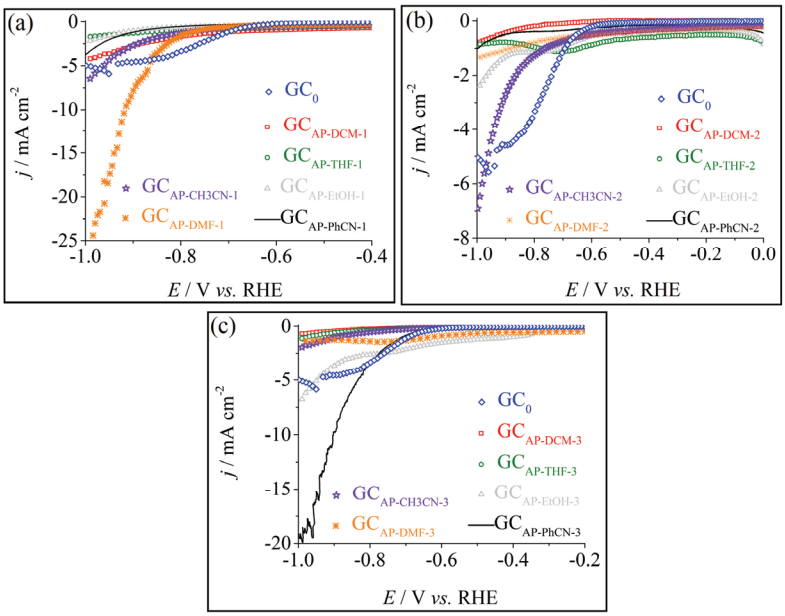

Fig. 1. Cathodic LSVs obtained on GC_0 and on: a) $GC_{AP\text{-}DCM\text{-}1}$, $GC_{AP\text{-}THF\text{-}1}$, $GC_{AP\text{-}EtOH\text{-}1}$, $GC_{AP\text{-}PhCN\text{-}1}$, $GC_{AP\text{-}CH3CN\text{-}1}$ and $GC_{AP\text{-}DMF\text{-}1}$; b) $GC_{AP\text{-}DCM\text{-}2}$, $GC_{AP\text{-}THF\text{-}2}$, $GC_{AP\text{-}EtOH\text{-}2}$, $GC_{AP\text{-}PhCN\text{-}2}$, $GC_{AP\text{-}CH3CN\text{-}2}$ and $GC_{AP\text{-}DMF\text{-}2}$; c) $GC_{AP\text{-}DCM\text{-}3}$, $GC_{AP\text{-}THF\text{-}3}$, $GC_{AP\text{-}EtOH\text{-}3}$, $GC_{AP\text{-}PhCN\text{-}3}$, $GC_{AP\text{-}CH3CN\text{-}3}$ and $GC_{AP\text{-}DMF\text{-}3}$. Electrolyte solution: 1 mol L^{-1} KOH; v = 5 mV s^{-1}.

Statistical analysis

The data collected during the electrochemical experiments carried out on the electrodes manufactured with the solution-based method were further exploited in statistical analysis. A correlation analysis was conducted to assess whether there is a significant relationship between the polarity of the organic solvents, the pH of the electrolyte solutions, and the number of layers drop-casted on the GC support on the one hand and the overpotential on the other. The only statistically significant correlation was obtained between the pH and the OER overpotential – $r_S(45)$ = = 0.447, $p < 0.01$ – indicating a medium association in the positive direction between the two parameters. The r_S^2 value specifies that approximately 20 % of

the variance in overpotential can be predicted from the pH. The correlation procedure is presented in the Supplementary material.

Experiments with electrodes obtained using the catalyst ink-based method

Fig. S-8 presents the anodic polarization curves recorded on the electrodes modified with the tetraazaporphyrin *via* the catalyst ink-based method. In all cases the unmodified GC electrode and the electrode manufactured using a catalyst ink containing only carbon black as the dispersed phase (GC_{CB}) are more electrocatalytically active compared with the modified specimens. The data collected during the HER investigation is shown in Fig. 2. GC_{CB} is more electrocatalytically active in the acidic and neutral environments (Fig. 2a and b), but the GC_{AP} and GC_{CB-AP} electrodes are significantly more active in the strongly alkaline solution (Fig. 2c). GC_{CB-AP} exhibits the highest water-splitting electrocatalytic activity found during the electrochemical experiments: $\eta_{HER} = 0.6$ V at $j = -10$ mA cm^{-2}.

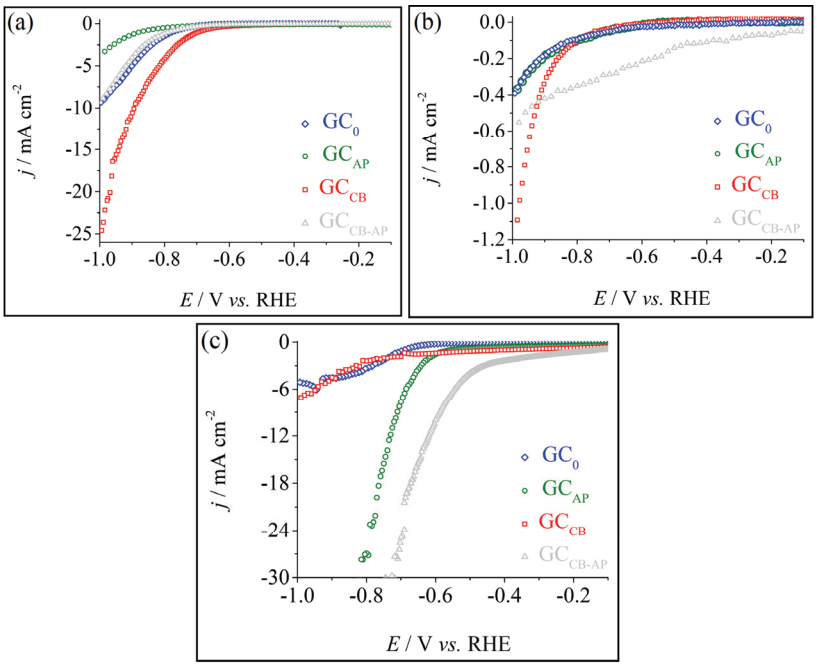

Fig. 2. Cathodic LSVs obtained on GC_0, GC_{CB}, GC_{AP} and GC_{CB-AP} in the following electrolyte solutions: a) 0.1 mol L^{-1} H_2SO_4, b) 0.1 mol L^{-1} KCl and c) 1 mol L^{-1} KOH; $v = 5$ mV s^{-1}.

The most active specimen was the focus of additional investigations aimed at outlining more of its water-splitting catalytic properties. The voltammetric and chronoamperometric data acquired during these experiments can be seen in Fig. 3. The electroactive surface area (*ECSA*) of the electrode was calculated based on the

value of the electric double-layer capacitance (C_{dl}), which is equal to the absolute value of the slope of the curve drawn by plotting the capacitive current density (j_{dl}) *vs.* the scan rate. Fig. 3a shows the graphical representation of two curves obtained for two GC_{CB-AP} specimens. The j_{dl} values were calculated with Eq. (S-5) using data from the cyclic voltammograms recorded at increasing scan rate values and presented in Fig. S-9 of the Supplementary material.[41] The curves from Fig. 3a are almost overlapping and the average value of their slopes (C_{dl}) can be found in Table III together with the values of other electrochemical parameters calculated in the study: the roughness factor (R_f) and *ECSA*. R_f is the ratio between the real surface of an electrode and its geometrical surface and is determined by dividing C_{dl} to the specific capacitance of a smooth electrode surface (C_s = 0.06 mF cm^{-2}).[42] Eq. (S-6) was employed to estimate the *ECSA* value.[43] This parameter is important in water-splitting studies due to its direct proportionality to the number of active sites involved in water electrolysis and also because it is used to investigate the OER and HER kinetics.[44–46]

TABLE III. The C_{dl}, R^2, R_f and *ECSA* values determined for the GC_{CB-AP} electrode

Electrode	C_{dl} / mF cm^{-2}	R^2	R_f	*ECSA* / cm^2
GC_{CB-AP}	1.416	0.9974	23.6	6.608

The HER kinetics at the interface between GC_{CB-AP} and the 1 mol L^{-1} KOH electrolyte solution were investigated as well. Fig. 3b shows the Tafel plot used to determine the Tafel slope, which in the present case was found to be 0.15 V dec^{-1} (R^2 = 0.9994). A low value of this parameter is preferable because it indicates faster reaction kinetics, but in strongly alkaline environments the surface of the working electrode can become covered to a large extent with hydrogen bubbles, leading to an increased slope value. When the slope is in the 0.04–0.12 V dec^{-1} range, the hydrogen evolution unfolds along a Volmer–Heyrovsky mechanism and the rates of the discharge and desorption steps are comparable, but in cases in which the slope is > 0.12 V dec^{-1} due to the high pH of the environment, a Volmer--limited mechanism is likely to unfold and the rate of the Heyrovsky step becomes slower than that of the Volmer step.[47–49]

The electrochemical stability of the GC_{CB-AP} electrode was also evaluated, with the results being presented in Fig. 3c. The chronoamperogram was recorded during a 7-hour period while maintaining constant the potential value corresponding to j = –10 mA cm^{-2}. Subsequently, a cathodic polarization curve was traced to evaluate the electrode's HER electrocatalytic activity and it is compared with the one obtained before the experiment (inset to Fig. 3c). The shape of the two LSVs is similar and an increase in the HER overpotential of just 14 mV is observed at j = –10 mA cm^{-2}. The electrode was analyzed by Raman Spectroscopy as well. Fig. S-10 of the Supplementary material shows the Raman spectra for the sample

before and after the stability test. The signals observed on the spectrum before the experiment are also observed on the one traced afterward. This result is evidence that the GC_{CB-AP} electrode did not undergo any significant structural modifications.

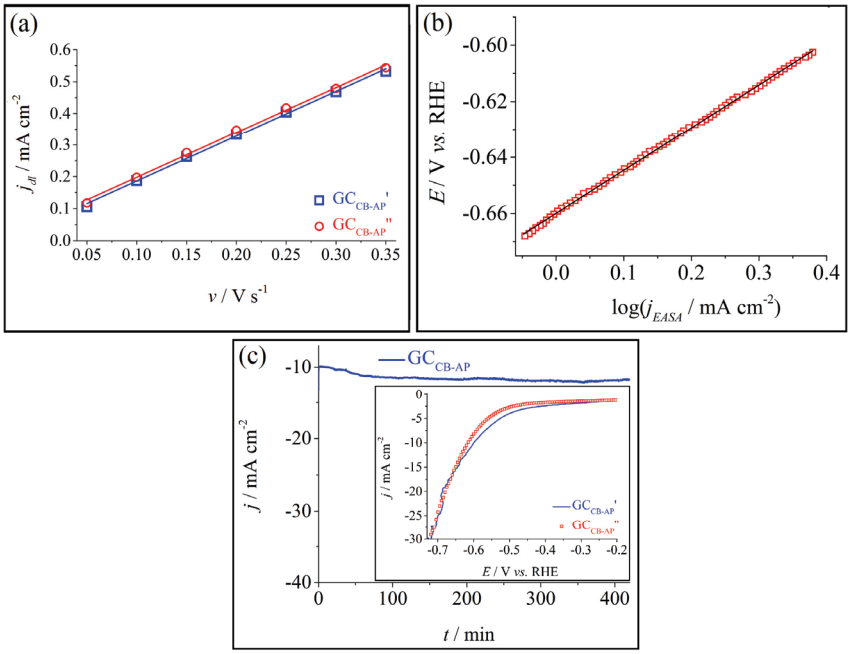

Fig. 3. a) The capacitive current density *vs.* scan rate plots obtained for two GC_{CB-AP} electrodes. b) Tafel plot for GC_{CB-AP} in 1 mol L^{-1} KOH solution. The current density (j_{ECSA}) was *ECSA*-normalized. c) Current density *vs.* time curve recorded on GC_{CB-AP} in 1 mol L^{-1} KOH solution and inset showing the polarization curves traced on GC_{CB-AP} before (GC_{CB-AP}') and after (GC_{CB-AP}'') the chronoamperometric experiment (1 mol L^{-1} KOH solution, v = 5 mV s^{-1}).

Considerations about the HER activity of the GC_{CB-AP} electrode

The GC_{CB-AP} sample obtained by employing the catalyst ink-based method displays the highest HER catalytic activity among the investigated specimens. It has been reported that the catalytic center of porphyrinoids is located in their macrocycle, more specifically at the N_4 site in case of the free-base compounds and the M-N_4 site in case of the metalated ones.[50–52] Since the tetraazaporphyrin used to modify the GC support is metal-free, its catalytic center is probably located at the N_4 site of its porphyrin-derived macrocycle. The previously mentioned relationship between ECSA and the number of active sites involved in the electrocatalytic process implies that a higher value of the former parameter corresponds

to a larger number of catalytic centers. GC_{CB-AP}'s ECSA (of 6.608 cm^2) is considerably higher than its geometric surface (of 0.28 cm^2), which points to a relatively high number of such centers. Porphyrinoid-modified electrodes exhibiting electrocatalytic activity, as is the case with GC_{CB-AP}, possess catalytic properties arising from surface structural features, increased π-resonance and charge transport phenomena.[53] One way in which charge transport unfolds is *via* π–π interactions between adjacent porphyrazine molecules, but the interface between the electrocatalyst and the conductive GC support is also involved. Because the nitrogen atoms located in the tetraazaporphyrin's macrocycle display higher electronegativity compared with the GC's carbon atoms, an electropositive doping effect is induced on the substrate's surface.[50] At the molecular level, the electron transport depends on the relationship between the macrocycle and its peripheral substituents, and the electronic effects of the substituents have an impact on the electrocatalytic water-splitting properties of porphyrinoids.[54] The tert-butyl moieties of the tetraazaporphyrin used to manufacture the GC_{CB-AP} electrode are electron-donating. As for the carbon black particles that were mixed with the porphyrazine to obtain the catalyst ink, their purpose is to improve the charge transport during water electrolysis. Basically, some of GC_{CB-AP}'s features have a positive impact on its catalytic activity (the relatively large number of catalytic centers, the electropositive doping effect of the GC and the carbon black particles), while others have a negative effect (the substituents' electron-donating effect). These characteristics and the electrolyte solution's high pH, whose influence on the Tafel slope has already been mentioned, are responsible for the electrode's HER activity. In Table IV this activity is compared to that of other porphyrinoid-based electrodes.

The η_{HER} and Tafel slope values are lower than some of the values from the table and are comparable to some of the remaining ones. The GC_{CB-AP} electrode displays higher electrocatalytic activity compared to electrodes modified with an A_3B Zn-porphyrin, a Co-phthalocyanine-based nanohybrid, amines-substituted Co-corroles, Fe- and Ni-porphyrin polymers, and a Co oxytyramine phthalocyanine polymer.[27,57,66–68] Also, the electrocatalytic activity of GC_{CB-AP} is similar to that of an electrode modified with a Zn-porphyrin–ferrocene imine gel and an imidazolyl-substituted free base porphyrin coated on carbon nanotubes. [59,64] In other words, the porphyrinoid-based electrocatalysts exhibiting lower or comparable activity to the tetraazaporphyrin studied herein belong to several compound classes - metallated and free base porphyrinoids, polymers and hybrids. Regarding the Tafel slopes, out of the 29 values reported in the literature and mentioned in the Table, 9 are higher than the value found for GC_{CB-AP} and 7 are comparable to it. This result is more than acceptable considering the simplicity of the manufacturing method used to obtain the electrode. More complex methods, such as the ones involving pulsed laser deposition, could further evidence the electrocatalyst's potential.

TABLE IV. The HER activity of GC_{CB-AP} and of other porphyrinoid-based electrodes studied in 1 mol L^{-1} KOH. The η_{HER} values are read at $j = -10$ mA cm^{-2}

Electrocatalyst or electrode	Substrate	η_{HER} / mV	Tafel slope, mV dec^{-1}	Ref.
Cu-CMP700	GC	430	167	55
Cu-CMP800	GC	380	135	55
Cu-CMP850	GC	350	135	55
Cu-CMP900	GC	430	135	55
CoP-2ph-CMP-800	GC	360	121	56
CoP-3ph-CMP-800	GC	380	–	56
CoP-4ph-CMP-800	GC	440	–	56
CoPc@MCA	GC	707	124	57
CoPc	GC	599	123	57
TiCP-PCP	Carbon fiber paper	310	–	58
ZnTAPP-NA	GC	546	121	59
CoTAPP-NA	GC	470	110	59
CoTPP-SD	Carbon fiber paper	475	–	60
CoCOP	Carbon fiber paper	310	161	60
PyCoPc/GO	GC	373	145	61
PyCoPc/GO-800	GC	253	96	61
CoPor-GDY	Carbon cloth	308	129	62
$G_{ZnP-DMF-1}$	Graphite	520	150	63
H_2TIPP@CNT-2	GC	599	127.6	64
CoTIPP@CNT-2	GC	485	102.3	64
NiTIPP@CNT-2	GC	529	104	64
CoTAPPCC	Ni foam	210	116	65
$G_{P4-NiPh-THF}$	Graphite	430	140	44
Co(tpfpc)	Carbon paper	960	275	66
Co(ttfphc)	Carbon paper	900	218	66
Co(ttfpdc)	Carbon paper	860	214	66
Fe-porphyrin polymer	Carbon paper	678	363	67
Co-porphyrin polymer	Carbon paper	437	195	67
Ni-porphyrin polymer	Carbon paper	644	345	67
Cu-porphyrin polymer	Carbon paper	436	236	67
Poly[CoOTPc]+KB	GC	390	80	68
Poly[CoOTPc]	GC	515	98	68
GC_{P1-CB}	GC	770	135	27
GC_{CB-AP}	GC	600	150	This work

CONCLUSION

A symmetrically substituted tetraazaporphyrin was tested as water-splitting electrocatalyst in a wide pH range. The electrodes modified with this porphyrazine were manufactured using two different methods. The best results were observed for the GC_{CB-AP} electrode obtained with the catalyst ink-based method. In strong alkaline medium it exhibits a η_{HER} value of 0.6 V (at $j = -10$ mA cm^{-2}) and a Tafel slope of 0.15 V dec^{-1}. The water electrolysis data collected by testing the electrodes modified with the solution-based method were used in statistical analysis,

which revealed a statistically significant correlation between the pH and the OER overpotential. Furthermore, the porphyrazine was investigated in gas phase by performing quantum chemical calculations. Overall, the three hybrid-DFT methods yielded comparable values for the key parameters of the molecular structure.

The results derived from experimental and theoretical approaches may function as a foundation from which extensive studies can be initiated, including the modeling of the chemistry and thermodynamics of redox processes and electron transfer, or more complex reaction mechanisms such as solute diffusion or surface diffusion.

The present work outlines the tetraazaporphyrin's applicative potential in the water-splitting domain and contributes to improving the current understanding of its features.

SUPPLEMENTARY MATERIAL

Additional data and information are available electronically at the pages of journal website: https://www.shd-pub.org.rs/index.php/JSCS/article/view/13305, or from the corresponding author on request.

Acknowledgements. The authors would like to thank Dr. Eugenia Fagadar-Cosma for the purchasing and providing of the porphyrazine and Dr. Florina Stefania Rus from INCEMC Timisoara (Romania) for performing the Raman analysis.

ИЗВОД

ЕЛЕКТРОКАТАЛИТИЧКА СВОЈСТВА ЗА РАЗЛАГАЊЕ ВОДЕ И РАЧУНАРСКА КАРАКТЕРИЗАЦИЈА СИМЕТРИЧНО СУПСТИТУИСАНОГ ПОРФИРАЗИНА

MARINA ALEXANDRA TUDORAN и BOGDAN-OVIDIU TARANU

National Institute of Research and Development for Electrochemistry and Condensed Matter, Dr. A. Paunescu Podeanu Street No. 144, 300569 Timisoara, Romania

Порфиразин 2,7,12,17-тетра-*трет*-бутил-5,10,15,20-тетрааза-21*H*,23*H*-порфин је испитиван у погледу његове електрокаталитичке активности разлагања воде у широком pH опсегу. За производњу електрода на бази овог једињења коришћене су две различите методе: метода заснована на раствору и метода заснована на суспензији катализатора. Каталитички најактивнија електрода је добијена методом заснованом на суспензији катализатора. У раствору KOH концентрације 1 mol L^{-1} ова електрода показује пренапетост реакције издвајања H_2 од 0,6 V и Тафелов нагиб од 0,15 V dec^{-1}. Статистичка анализа је показала значајну корелацију између pH и пренапетости реакције издвајања O_2. Квантно-хемијски прорачуни су извршени како би се добило детаљније разумевање својстава порфиразина.

(Примљено 23. марта, ревидирано 19. јуна, прихваћено 10. јула 2025)

REFERENCES

1. G. Singh, S. Chandra, *Electrochem. Sci. Adv.* **3** (2023) e2100149 (https://doi.org/10.1002/elsa.202100149)
2. A. Ghosh, J. Fitzgerald, P. G. Gassman, J. Almlof, *Inorg. Chem.* **33** (1994) 6057 (https://doi.org/10.1021/ic00104a014)

3. P. A. Pinheiro, G. F. M. Pereira, L. O. Cunha, J. P. S. C. Leal, M. E. Alvarenga, F. T. Martins, H. Silva, J. L. S. Milani, T. T. Tasso, *Photochem. Photobio. Sci.* **23** (2024) 1757 (https://doi.org/10.1007/s43630-024-00629-z)
4. D.-P. Medina, J. Fernandez-Ariza, M. Urbani, F. Sauvage, T. Torres, M. S. Rodriguez--Morgade, *Molecules* **26** (2021) 2129 (https://doi.org/10.3390/molecules26082129)
5. T. Koczorowski, B. Wicher, R. Krakowiak, K. Mylkie, A. Marusiak, E. Tykarska, M. Ziegler-Borowska, *Materials* **15** (2022) 7264 (https://doi.org/10.3390/ma15207264)
6. H. N. Silva, S. H. Toma, A. L. Hennemann, J. M. Goncalves, M. Nakamura, K. Araki, M. M. Toyama, H. E. Toma, *Molecules* **27** (2022) 4598 (https://doi.org/10.3390/molecules27144598)
7. S. A. Lermontova, T. S. Lyubova, I. S. Grigoryev, V. A. Ilichev, V. I. Plekhanov, N. Y. Shilyagina, I. V. Balalaeva, V. P. Boyarskiy, L. G. Klapshina, *Russ. J. Gen. Chem.* **93** (2023) S672 (https://doi.org/10.1134/S1070363223160053)
8. A. M. Alsharari, A. A. A. Darwish, M. Rashad, *Opt. Mater.* **105** (2020) 109870 (https://doi.org/10.1016/j.optmat.2020.109870)
9. N. Kobayashi, S. Nakajima, H. Ogata, T. Fukuda, *Chem.-Eur. J.* **10** (2004) 6294 (https://doi.org/10.1002/chem.200400275)
10. S. Yamazaki, M. Asahi, N. Taguchi, T. Ioroi, *J. Electroanal. Chem.* **848** (2019) 113321 (https://doi.org/10.1016/j.jelechem.2019.113321)
11. I. Fringu, D. Anghel, I. Fratilescu, C. Epuran, M. Birdeanu, E. Fagadar-Cosma, *Biomedicines* **12** (2024) 770 (https://doi.org/10.3390/biomedicines12040770)
12. A. A. Al-Zubaidi, A. A. A. Elfaki, A. A. A. Darwish, *J. Mol. Struct.* **1218** (2020) 128499 (https://doi.org/10.1016/j.molstruc.2020.128499)
13. I. Slobodkin, E. Davydova, M. Sananis, A. Breytus, A. Rothschild, *Nat. Mater.* **23** (2024) 398 (https://doi.org/10.1038/s41563-023-01767-y)
14. N. S. Hassan, A. A. Jalil, S. Rajendran, N. F. Khusnun, M. B. Bahari, A. Johari, M. J. Kamaruddin, M. Ismail, *Int. J. Hydrogen Energy* **52** (2024) 420 (https://doi.org/10.1016/j.ijhydene.2023.09.068)
15. J. E. Lee, I. Shafiq, M. Hussain, S. S. Lam, G. H. Rhee, Y.-K. Park, *Int. J. Hydrogen Energy* **47** (2022) 4346 (https://doi.org/10.1016/j.ijhydene.2021.11.065)
16. H. Sun, X. Xu, H. Kim, W. Jung, W. Zhou, Z. Shao, *Energy Environ. Mater.* **6** (2023) e12441 (https://doi.org/10.1002/eem2.12441)
17. Y. Yao, J. Lyu, X. Li, C. Chen, F. Verpoort, J. Wang, Z. Pan, Z. Kou, *DeCarbon* **5** (2024) 100062 (https://doi.org/10.1016/j.decarb.2024.100062)
18. X. Xie, L. Du, L. Yan, S. Park, Y. Qiu, J. Sokolowski, W. Wang, Y. Shao, *Adv. Funct. Mater.* **32** (2022) 2110036 (https://doi.org/10.1002/adfm.202110036)
19. C. Tian, R. Liu, Y. Zhang, W. Yang, B. Wang, *Nano Res.* **17** (2024) 982 (https://doi.org/10.1007/s12274-023-6003-5)
20. N. A. Kamaruzaman, W. M. K. W. M. Zin, K. H. Kamarudin, N. M. Saleh, F. Yusoff, *Int. J. Electrochem. Sc.* **18** (2023) 100187 (https://doi.org/10.1016/j.ijoes.2023.100187)
21. Y. Chen, X. Zhao, P. Dong, Y. Zhang, Y. Zou, S. Wang, *New Carbon Mater.* **39** (2024) 1 (https://doi.org/10.1016/S1872-5805(24)60831-0)
22. E. Nikoloudakis, A. G. Coutsolelos, E. Stratakis, *Energy Fuel* **38** (2024) 19222 (https://doi.org/10.1021/acs.energyfuels.4c03322)
23. L. R. Snyder, J. J. Kirkland, J. L. Glajch, *Practical HPLC Method Development*, John Wiley & Sons, Hoboken, NJ, 1997 (https://doi.org/10.1002/9781118592014)
24. Z. Szabadai, L. Sbarcea, L. Udrescu, *Analiza fizică și chimică a medicamentului*, Victor Babes publishing house, Timisoara, 2016 (ISBN 978-606-786-020-7)

25. W. Szczolko, T. Koczorowski, B. Wicher, M. Kryjewski, Z. Krakowska, E. Tykarska, T. Goslinski, *Dyes Pigments* **206** (2022) 110607 (https://doi.org/10.1016/j.dyepig.2022.110607)
26. E. Gonca, *J. Coord. Chem.* **70** (2017) 2344 (https://doi.org/10.1080/00958972.2017.1350267)
27. B.-O. Taranu, F. S. Rus, E. Fagadar-Cosma, *Coatings* **14** (2024) 1 (https://doi.org/10.3390/coatings14081048)
28. J. Chang, Q. Lv, G. Li, J. Ge, C. Liu, W. Xing, *Appl. Catal., B* **204** (2017) 486 (https://doi.org/10.1016/j.apcatb.2016.11.050)
29. Y. Ge, Z. Lyu, M. Marcos-Hernandez, D. Villagran, *Chem. Sci.* **13** (2022) 8597 (https://doi.org/10.1039/D2SC01250B)
30. B.-R. Wulan, S.-S. Yi, S.-J. Li, Y.-X. Duan, J.-M. Yan, X.-B. Zhang, Q. Jiang, *Mater. Chem. Front.* **2** (2018) 1799 (https://doi.org/10.1039/C8QM00239H)
31. A. Raveendran, M. Chandran, R. Dhanusuraman, *RSC Adv.* **13** (2023) 3843 (https://doi.org/10.1039/D2RA07642J)
32. O. van der Heijden, S. Park, R. E. Vos, J. J. J. Eggebeen, M. T. M. Koper, *ACS Energy Lett.* **9** (2024) 1871 (https://doi.org/10.1021/acsenergylett.4c00266)
33. M. K. Mongale, D. A. Isabirye, M. M. Kabanda, T. O. Aiyelabola, E. E. Ebenso, *Asian J. Chem.* **29** (2017) 496 (https://doi.org/10.14233/ajchem.2017.20205)
34. J. H. Luo, Q. S. Li, L. N. Yang, Z. Z. Sun, Z. S. Li, *RSC Adv.* **4** (2014) 20200 (https://doi.org/10.1039/C4RA02204A)
35. M. E. Ayalew, *J. Biophys. Chem.* **13** (2022) 29 (https://doi.org/10.4236/jbpc.2022.133003)
36. K. Arumugam, U. Becker, *Minerals* **4** (2014) 345 (https://doi.org/10.3390/min4020345)
37. S. Sarfaraz, M. Yar, A. Hussain, A. Lakhani, A. Gulzar, M. Ans, U. Rashid, M. Hussain, S. Muhammad, I. Bayach, N.S. Sheikh, K. Ayub, *ACS Omega* **8** (2023) 36493 (https://doi.org/10.1021/acsomega.3c05477)
38. S. Sarfaraz, M. Yar, N. S. Sheikh, I. Bayach, K. Ayub, *ACS omega* **8** (2023) 14077 (https://doi.org/10.1021/acsomega.3c00721)
39. V. K. Kumar, R. Sangeetha, D. Barathi, R. Mathammal, N. Jayamani, *Spectrochim. Acta, A* **118** (2014) 663 (https://doi.org/10.1016/j.saa.2013.08.089)
40. X. Li, Y. Du, L. Ge, C. Hao, Y. Bai, Z. Fu, Y. Lu, Z. Cheng, *Adv. Funct. Mater.* **33** (2023) 1 (https://doi.org/10.1002/adfm.202210194)
41. B. O. Taranu, S. D. Novaconi, M. Ivanovici, J. N. Goncalves, F. S. Rus, *Appl. Sci. (Basel)* **12** (2022) 6821 (https://doi.org/10.3390/app12136821)
42. M. L. F. Ciriaco, M. I. Silva-Pereira, M. R. Nunes, F. M. Costa, *Port. Electrochim. Acta* **17** (1999) 149 (https://doi.org/10.4152/pea.199902149)
43. A. Karmakar, S. Kundu, *Mater. Today Energy* **33** (2023) 1 (https://doi.org/10.1016/j.mtener.2023.101259)
44. B.-O. Taranu, E. Fagadar-Cosma, P. Sfirloaga, M. Poienar, *Energies* **16** (2023) 1 (https://doi.org/10.3390/en16031212)
45. B.-O. Taranu, P. Vlazan, P. Svera, M. Poienar, P. Sfirloaga, *J. Alloy. Compd.* **892** (2021) 162239 (https://doi.org/10.1016/j.jallcom.2021.162239)
46. M. Poienar, P. Svera, B.-O. Taranu, C. Ianasi, P. Sfirloaga, G. Buse, P. Veber, P. Vlazan, *Crystals* **12** (2022) 1803 (https://doi.org/10.3390/cryst12121803)
47. C. Wan, Y. Ling, S. Wang, H. Pu, Y. Huang, X. Duan, *ACS Central Sci.* **10** (2024) 658 (https://doi.org/10.1021/acscentsci.3c01439)

48. F. Bao, E. Kemppainen, I. Dorbandt, R. Bors, F. Xi, R. Schlatmann, R. van de Krol, S. Calnan, *ChemElectroChem* **8** (2021) 195 (https://doi.org/10.1002/celc.202001436)
49. Z. Y. Wu, B. C. Hu, P. Wu, H. W. Liang, Z. L. Yu, Y. Lin, Y. R. Zheng, Z. Li, S. H. Yu, *NPG Asia Mater.* **8** (2016) e288 (https://doi.org/10.1038/am.2016.87)
50. S. Seo, K. Lee, M. Min, Y. Cho, M. Kim, H. Lee, *Nanoscale* **9** (2017) 3969 (https://doi.org/10.1039/c6nr09428g)
51. W. Zhang, W. Lai, R. Cao, *Chem. Rev.* **117** (2017) 3717 (https://doi.org/10.1021/acs.chemrev.6b00299)
52. A. Facchin, C. Durante, *Adv. Sustain. Syst.* **6** (2022) 2200111 (https://doi.org/10.1002/adsu.202200111)
53. B. O. Taranu, E. Fagadar-Cosma, *Processes* **10** (2022) 611 (https://doi.org/10.3390/pr10030611)
54. B.-O. Taranu, *J. Serb. Chem. Soc.* **90** (2025) 447 (https://doi.org/10.2298/JSC241004105T)
55. S. Cui, M. Qian, X. Liu, Z. Sun, P. Du, *ChemSusChem* **9** (2016) 2365 (https://doi.org/10.1002/cssc.201600452)
56. H. Jia, Y. Yao, Y. Gao, D. Lu, P. Du, *Chem. Commun.* **52** (2016) 13483 (https://doi.org/10.1039/C6CC06972J)
57. J. Liu, C. Wang, H. Sun, H. Wang, F. Rong, L. He, Y. Lou, S. Zhang, Z. Zhang, M. Du, *Appl. Catal., B* **279** (2020) 1 (https://doi.org/10.1016/j.apcatb.2020.119407)
58. A. Wang, L. Cheng, X. Shen, W. Zhu, L. Li, *Dyes Pigments* **181** (2020) 1 (https://doi.org/10.1016/j.dyepig.2020.108568)
59. G. Cai, L. Zeng, L. He, S. Sun, Y. Tong, J. Zhang, *Chem. Asian J.* **15** (2020) 1963 (https://doi.org/10.1002/asia.202000083)
60. A. Wang, L. Cheng, W. Zhao, X. Shen, W. Zhu, *J. Colloid Interf. Sci.* **579** (2020) 598 (https://doi.org/10.1016/j.jcis.2020.06.109)
61. L. Chen, R. U. R. Sagar, J. Chen, J. Liu, S. Aslam, F. Nosheen, T. Anwar, N. Hussain, X. Hou, T. Liang, *Int. J. Hydrogen Energy* **46** (2021) 19338 (https://doi.org/10.1016/j.ijhydene.2021.03.075)
62. Q. Pan, X. Chen, H. Liu, W. Gan, N. Ding, Y. Zhao, *Mater. Chem. Front.* **5** (2021) 4596 (https://doi.org/10.1039/D1QM00285F)
63. B.-O. Taranu, E. Fagadar-Cosma, *Nanomaterials (Basel)* **12** (2022) 1 (https://doi.org/10.3390/nano12213788)
64. Y. Wang, D. Song, J. Li, Q. Shi, J. Zhao, Y. Hu, F. Zeng, N. Wang, *Inorg. Chem.* **61** (2022) 10198 (https://doi.org/10.1021/acs.inorgchem.2c01415)
65. Y. Dou, X. Yang, Q. Wang, Z. Yang, A. Wang, L. Zhao, W. Zhu, *J. Colloid Interf. Sci.* **644** (2023) 256 (https://doi.org/10.1016/j.jcis.2023.04.082)
66. S. Sahoo, E. K. Johnson, X. Wei, S. Zhang, C. W. Machan, *Energy Adv.* **3** (2024) 2280 (https://doi.org/10.1039/D4YA00257A)
67. N. Ocuane, Y. Ge, C. Sandoval-Pauker, D. Villagran, *Dalton Trans.* **53** (2024) 2306 (https://doi.org/10.1039/D3DT03371F)
68. N. Kousar, Giddaerappa, L. K. Sannegowda, *Int. J. Hydrogen Energy* **50** (2024) 37 (https://doi.org/10.1016/j.ijhydene.2023.06.296).